Supporting information

Polyoxometalate-Based {Mn^{III}_2}-Schiff Base Composite Materials Exhibiting Single-Molecule Magnet Behaviour

Qiong Wu, Yang-Guang Li,* Yong-Hui Wang, Rodolphe Clérac,* Ying Lu, and En-Bo Wang*

Contents:

1- Experimental Section

Materials and methods. All chemicals were commercially purchased and used without further purification. The staring materials $[Mn(salen)(H_2O)]_2(ClO_4)_2{\cdot}H_2O$, $Na_3[AlMo_6(OH)_6O_{18}]$ and $Na_3[CrMo_6(OH)_6O_{18}]$ were synthesized according to the literatures[1-3] and characterized by IR spectra. Elemental analyses Cr, Al, Mn and Mo were analyzed on a PLASMA-SPEC (I) ICP atomic emission spectrometer; C and N were performed on a Perkin-Elmer 2400 CHN elemental analyzer. IR spectra were recorded in the range 400-4000 cm^{-1} on an Alpha Centaurt FT/IR Spectrophotometer using KBr pellets. TG analyses were performed on a Perkin–Elmer TGA7 instrument in flowing N_2 with a heating rate of 10 $°C{\cdot}min^{-1}$. The magnetic susceptibility measurements were obtained with the use of a Quantum Design SQUID magnetometer MPMS-XL housed at the Centre de Recherche Paul Pascal. This magnetometer works between 1.8 and 400 K for dc applied fields ranging from -7 to 7 T. Measurements were performed on polycrystalline samples of 5.35, 19.78 and 30.47 mg for **1**, **2** and **3**, respectively. ac susceptibility measurements have been measured with an oscillating ac field of 3 Oe and ac frequencies ranging from 1 to 1500 Hz. It is worth mentioning that the relaxation times estimated above 1500 Hz have been obtained using a scaling technique on the frequency dependences of the ac susceptibility. The last temperature for which the maximum of the F(ν) plot is clearly observed in the available frequency window (1-1500 Hz) has been used as a reference and has been scaled on the available data when the maximum of the F(ν) plot is not observed. The magnetic data were corrected for the sample holder and the diamagnetic contributions.[4] *M* vs *H* measurements have been performed at 100 K to check for the presence of ferromagnetic impurities that has been found systematically absent.

X-ray Crystallography. The crystallographic data were collected at 150 K on the Rigaku R-axis Rapid IP diffractometer using graphite monochromatic Mo-Kα radiation (λ = 0.71073 Å) and IP technique. Multi-scan absorption correction was applied. The crystal data were solved by the direct method and refined by the full-matrix least-squares method on F^2 using the SHELXTL-97 crystallographic software package.[5] During the refinement, all the non-H atoms were anisotropically refined. H atoms on the C atoms were fixed on the calculated positions. H atoms on water molecules were found from the residual peaks and fixed on their mother O atoms with the restrained H-O bond distances. The H atoms on the disordered water molecules can not be determined from the difference Fourier maps and directly included in the final molecular formula. During the refinement, another restraint command “ISOR” was also used to refine the disordered solvent water molecules with ADP problems. This refinement led to a relative high restraint value of 69 for **1** and 63 for **2**. The highest residual peak and the deepest hole are 0.811 and -0.958 e $Å^{-3}$ for **1** and 0.667 and -0.775 e $Å^{-3}$ for **2**, respectively. The detailed crystal data and structure refinement for **1** and **2** were given in Table S1. Selected bond lengths and angles of **1** and **2** were listed in Table S2 and Table S3, respectively. Complex $[Mn_2(salen)_2(H_2O)_2](ClO_4)_2 \cdot H_2O$ (**3**) possesses a known crystal structure published in 1991 by Garcia-Deibe et al.[6]

Preparation of complexes 1 and 2: $Na_3[AlMo_6O_{24}H_6]$ (1.06 g, 1 mmol) was dissolved in 20 ml distilled water. Then, 20 ml methanol solution containing freshly prepared $[Mn(salen)(H_2O)]_2(ClO_4)_2 \cdot H_2O$ (0.88 g, 1 mmol) was quickly added to above solution. The dark-brown reaction mixture was sealed and stirred in a conical flask at 35 °C for 2 days. After filtration, the filtrate was slowly evaporated at room temperature. Dark-brown plate-like crystals of **1** were isolated in a week (yield 56.6 % based on Mo). Anal. $C_{32}H_{78}N_4O_{50}AlMn_2Mo_6Na$ **1**: C, 18.71; N, 2.73; Al, 1.31; Mn, 5.35; Mo, 28.01 %; Found: C, 18.93; N, 2.85; Al, 1.19; Mn, 5.24; Mo, 28.21 %. TG analysis confirms ca. 22 water molecules in complex **1**. Complex **2** was prepared with the same method except that $Na_3[CrMo_6O_{24}H_6]$ (1.09 g, 1 mmol) was used as the starting materials and the yield of the crystals of **2** is ca. 59.1 % based on Mo. Anal. $C_{32}H_{78}N_4O_{50}CrMn_2Mo_6Na$ **2**: C,18.48; N, 2.69; Cr, 2.50; Mn, 5.28; Mo, 27.68 %; Found: C, 18.71; N, 2.75; Cr, 2.32; Mn, 5.21; Mo, 27.94 %. TG analysis confirms ca. 22 water molecules in complex **2**.

Synthetic discussion. The reaction between $[Mn(salen)(H_2O)_2]_2(ClO_4)_2$ and Anderson-type POMs $Na_3[XMo_6(OH)_6O_{18}]$ (X =Al or Cr) in the mixed methanol-water solution led to the isolation of complexes **1** and **2**. During the preparation, the main difficulty is to choose suitable solvent media to make possible the reactions between $\{Mn^{III}_2\}$-salen complexes and POMs. Considering the POMs $Na_3[XMo_6(OH)_6O_{18}]$ were synthesized in aqueous solution and dimeric Mn^{III}-salen complexes were isolated from the mixed methanol-water solution, therefore, the mixed methanol-water solution was employed into the reaction system. It is worth mentioning that a lot of brown precipitates appeared immediately after two precursors were mixed together, however, after a long reaction period (ca. 2 days) with vigorous stirring at 35 °C, all the precipitate was slowly dissolved and the reaction solution was clear again. The dark-brown plate-like crystals of complexes **1** and **2** were isolated in a week with high yields.

References

1 (a) H. Miyasaka, R. Clérac, T. Ishii, H.-C. Chang, S. Kitagawa and M. Yamashita, *J. Chem. Soc., Dalton Trans.*, 2002, 1528; (b) H.-L. Shyu, H.-H. Wei and Y. Wang, *Inorg. Chim. Acta*, 1999, **290**, 8.

2 V. *Shivaiah*, M. Nagaraju and *S. K. Das*, Inorg. Chem., *2003*, *42*, *6604*.

3 A. Perloff, *Inorg. Chem.*, 1970, **9**, 2228.

4 E. A. Boudreaux and L. N. Mulay, *Theory and Applications of Molecular Paramagnetism*, John Wiley and Sons, New York, 1976, pp. 491–495.

5 (a) G. M. Sheldrick, *SHELXL97, Program for Crystal Structure Refinement*; University of Göttingen, Germany, **1997**; (b) G. M. Sheldrick, *SHELXS97, Program for Crystal Structure Solution*; University of Göttingen, Germany, **1997**.

6. A. Garcia-Deibe, A. Sousa, M. R. Bermejo, P. P. MacRory, C. A. McAuliffe, R. G. Pritchard, M. Hellowell, *J. Chem. Soc., Chem. Commun.*, **1991**, 728.

2 Supplementary Structural Fig.s of 1 and 2

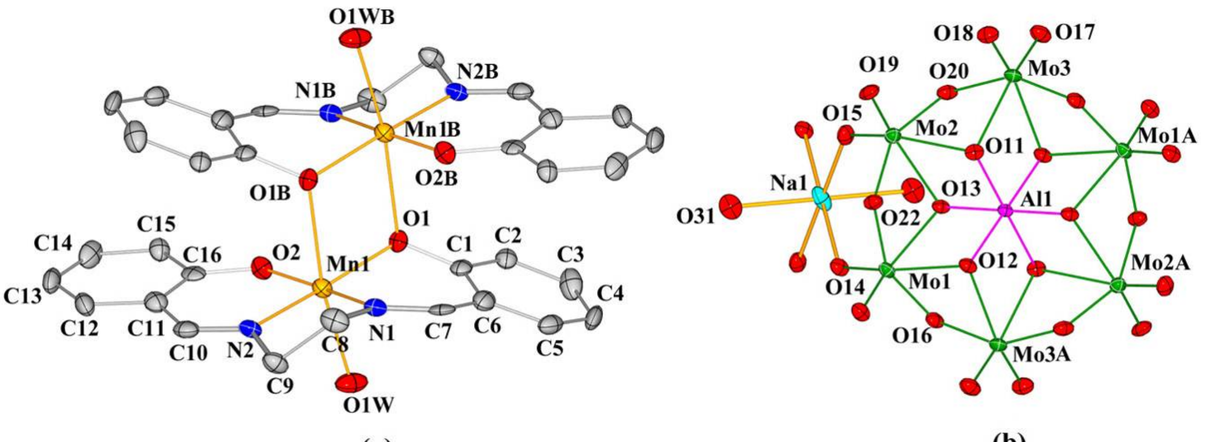

(a) (b)

Fig. S1. ORTEP diagram of complex **1** with the 50 % thermal ellipsoids for all the non-H atoms. The H atoms and solvent water molecules are omitted for clarity. (a) The cationic $[Mn(salen)(H_2O)]_2^{2+}$ fragment; (b) The anionic $[AlMo_6(OH)_6O_{18}]^{3-}$ moieties. Symmetry transformations used to generate equivalent atoms: A, -x+1,-y+1,-z+1; B, -x+2,-y+1,-z+2.

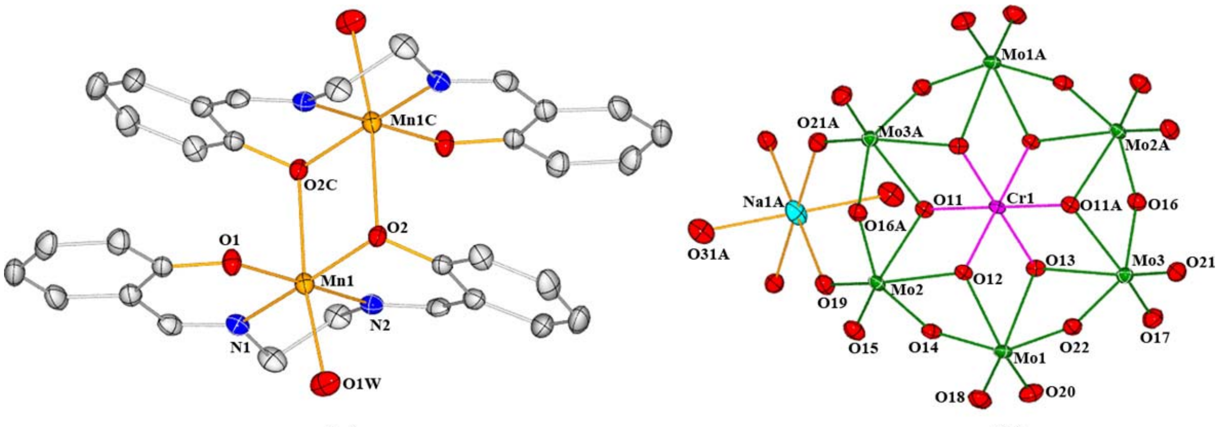

(a) (b)

Fig. S2. ORTEP diagram of complex **2** with the 50% thermal ellipsoids for all the non-H atoms. The H atoms and solvent water molecules are omitted for clarity. (a) The cationic $[Mn(salen)(H_2O)]_2^{2+}$ fragment; (b) The anionic $[CrMo_6(OH)_6O_{18}]^{3-}$ moieties. Symmetry transformations used to generate equivalent atoms: A, -x,-y,-z+1; C, -x+1,-y,-z+2.

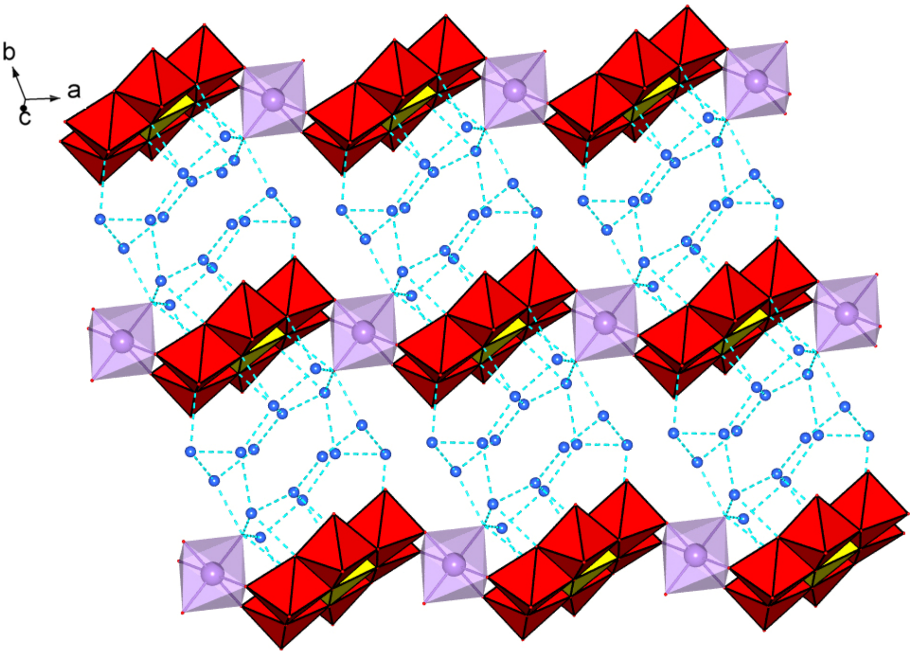

Fig. S3. The packing arrangement of **1** viewed along *c* axis, showing that all the 1-D chainlike $\{[Na(H_2O)_2][AlMo_6(OH)_6O_{18}]\}^{2-}$ polyoxoanions were linked by the $\{H_2O\}_{18}$ clusters into 2-D supramolecular inorganic network. H atoms on water molecules are omitted for clarity.

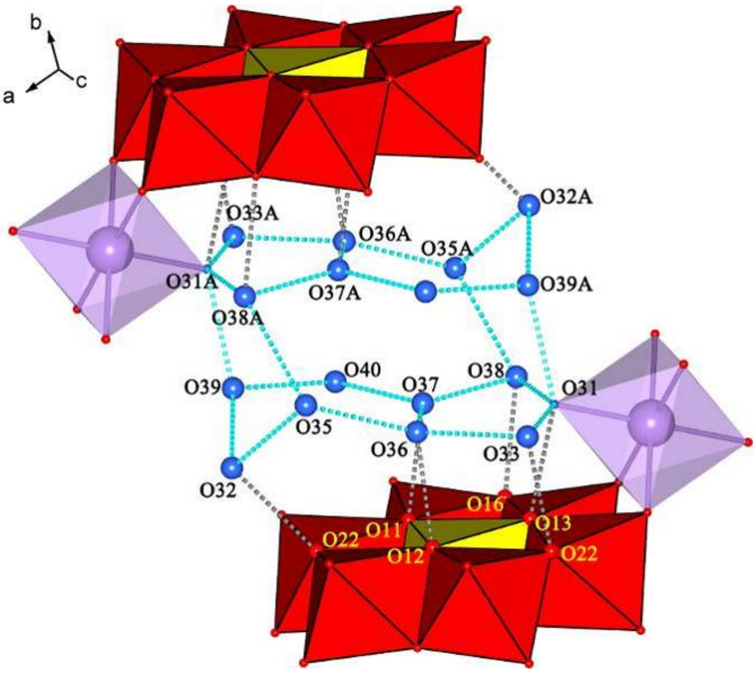

Fig. S4. View of the $\{H_2O\}_{18}$ cluster between two adjacent POM units in **1**. Detailed H-bonds are as follows: O31…O33, 2.812(8) Å; O32…O35, 2.781(8) Å; O37…O36, 2.701(1) Å; O38…O37, 2.836(1) Å; O38...O31, 3.131(9) Å; O35...O36, 2.766(8) Å; O35...O32, 2.781(8) Å; O39...O32, 3.238(1) Å; O39...O40, 2.841(1) Å; O40...O37, 2.840(9) Å; O31...O39A, 2.760(4) Å; O38...O35A, 3.001(1) Å; O32...O22, 2.781(7) Å; O33...O22, 2.781(8) Å; O37...O11, 2.733(1) Å; O31...O13, 2.779(7) Å; O36...O12 2.681(1) Å.

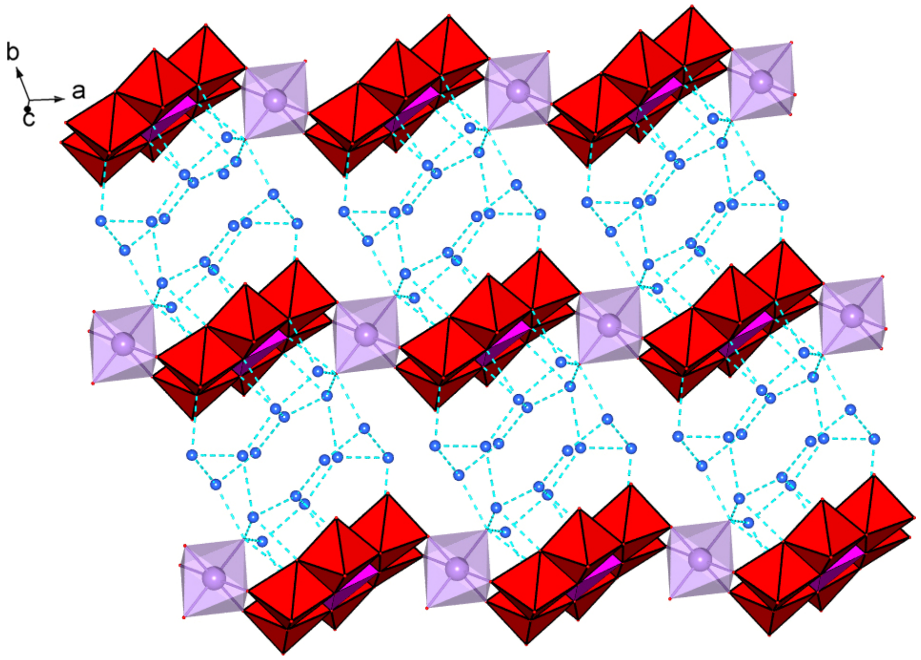

Fig. S5. The packing arrangement of **2** viewed along *c* axis, showing that all the 1-D chainlike $\{[Na(H_2O)_2][CrMo_6(OH)_6O_{18}]\}^{2-}$ polyoxoanions were linked by the $\{H_2O\}_{18}$ clusters into 2-D supramolecular inorganic network. H atoms on water molecules are omitted for clarity.

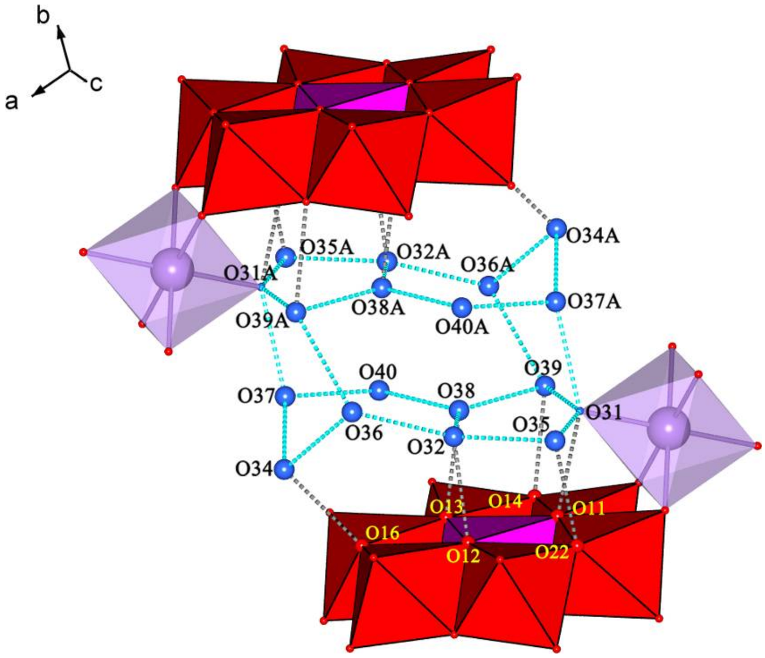

Fig. S6. View of the $\{H_2O\}_{18}$ cluster between two adjacent $\{CrMo_6\}$ POM units in **2**. The detailed H-bonds are as follows: O31…O35, 2.809(4) Å; O32…O35, 2.755(4) Å; O38…O32, 2.741(6) Å; O38…O39, 2.829(9) Å; O39...O31, 3.143(6) Å; O32...O36, 2.742(4) Å; O36...O34, 2.783(4) Å; O37...O34, 2.862(7) Å; O37...O40, 2.843(9) Å; O40...O38, 2.847(7) Å; O31...O37A, 2.746(6) Å; O39...O36A, 3.013(6) Å; O34...O16, 2.778(4) Å; O32...O12, 2.665(3) Å; O38...O13, 2.719(6) Å; O39...O14, 2.783(7) Å; O31...O11, 2.757(4) Å; O35...O22, 2.738(4) Å.

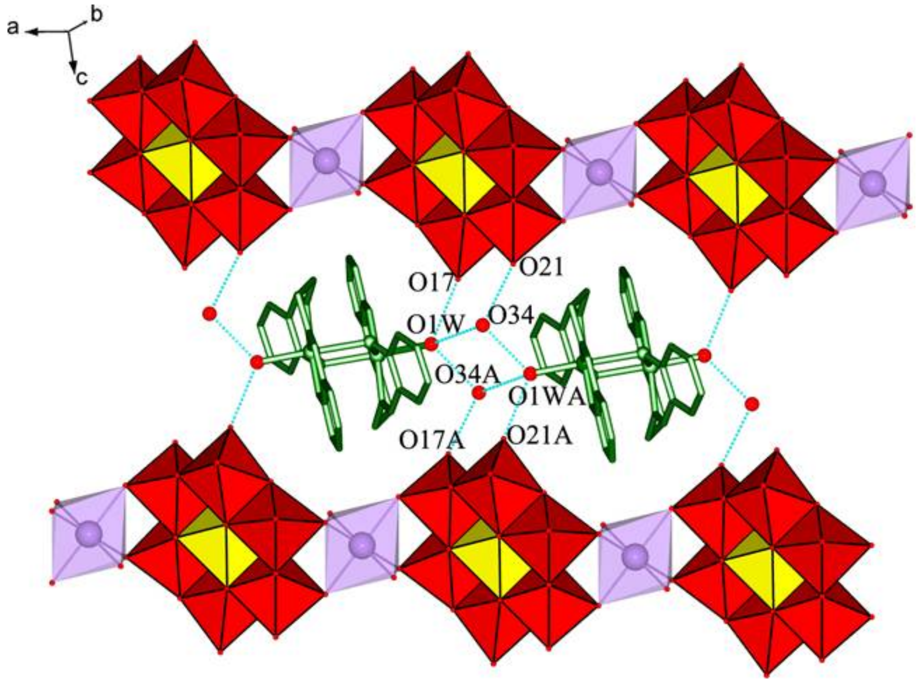

Fig. S7. View of the H-bonding interactions among {Mn_2} units, {$AlMo_6$} moieties and solvent water molecules in **1**. The detailed H-bonds are as follows: OW1…O34, 3.368 Å; O34…O21, 2.799 Å; OW1…O17, 2.838 Å.

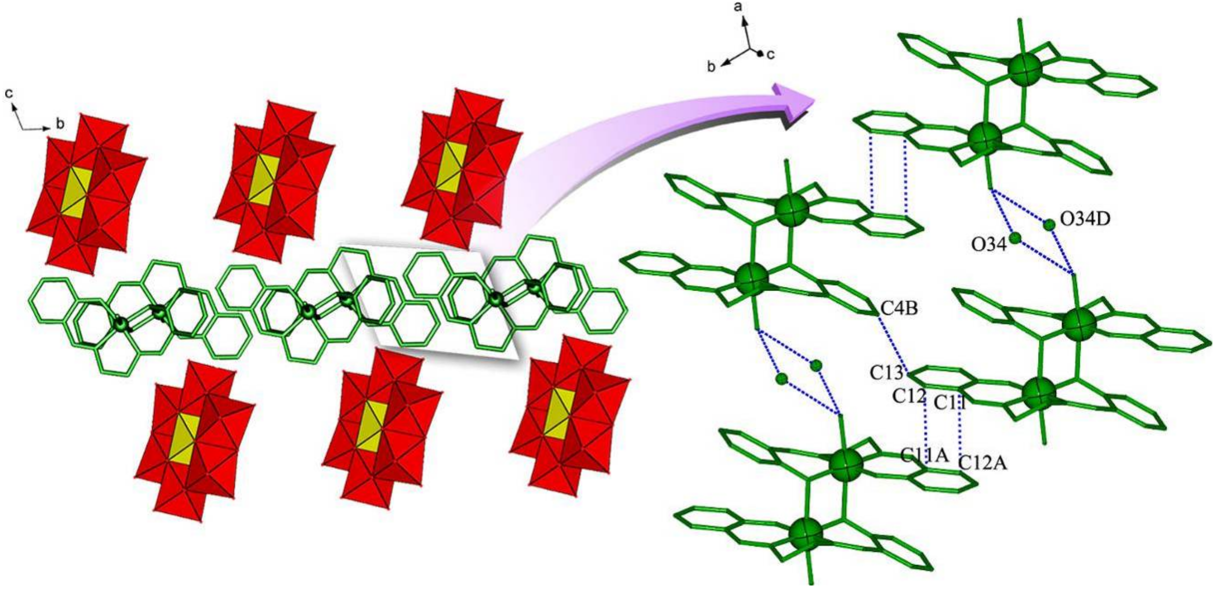

Fig. S8. (a) The packing arrangement of **1** viewed along *a* axis and **(b)** the C…C distance between adjacent salen ligands of the {Mn_2} dimeric units. The distance of C11…C12A is 3.451(2) Å, and the distance of C13… C4B is 3.458(7) Å. Symmetry transformations used to generate equivalent atoms: A: 2-x, 2-y, 2-z; B: 1+x, 1+y, z. Although the distances between two benzene planes are close, these planes are not overlapped at all, thus, there are no π-π interactions between two adjacent {Mn_2} dimers.

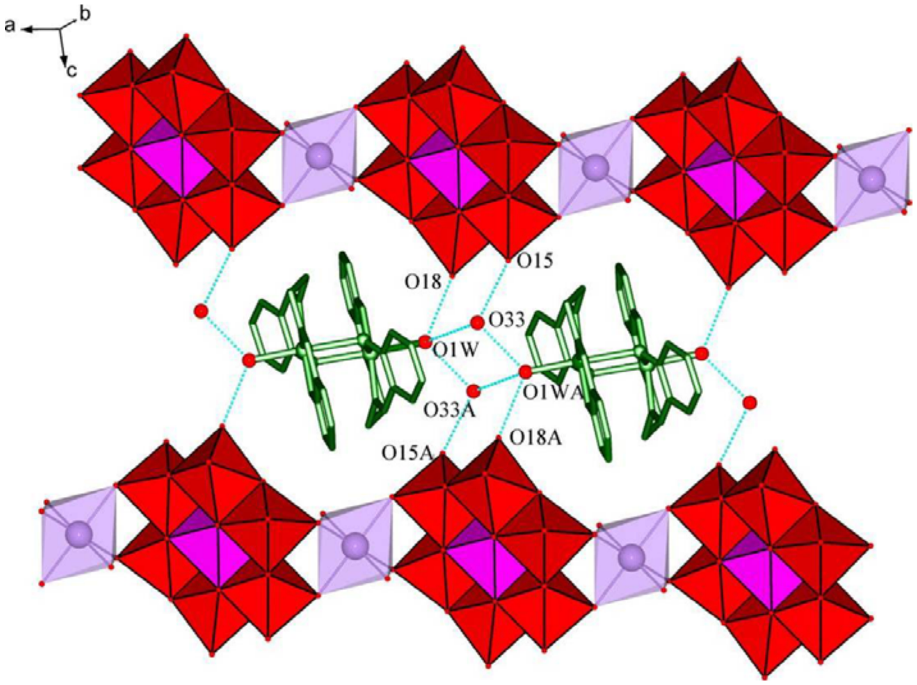

Fig. S9. View of the H-bond interactions among {Mn$_2$} units, {CrMo$_6$} moieties and solvent water molecules along ca. *b*-direction. The detailed H-bonds are as follows: O1W…O33, 2.712 Å; O33…O15, 2.801 Å; O1W…O18, 2.839 Å.

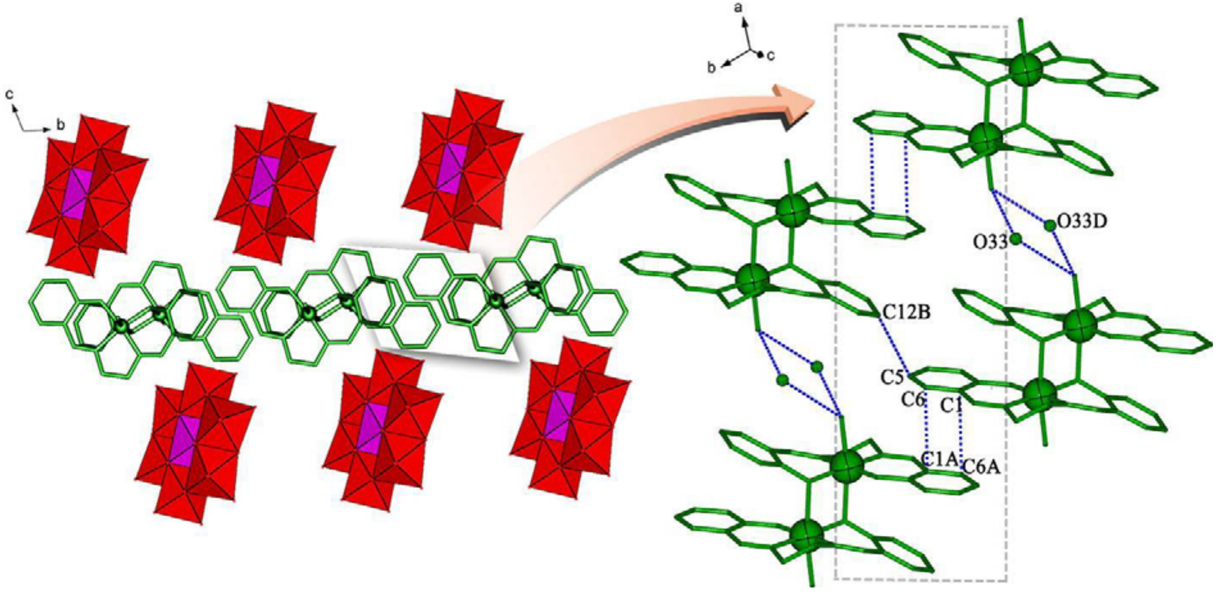

Fig. S10. (a) The packing arrangement of **2** viewed along *a* axis and **(b)** the C…C distance between adjacent salen ligands of the {Mn$_2$} dimeric units. The distance of C1…C6A is 3.473(2) Å, and the distance of C5… C12B is 3.481(7) Å. Symmetry transformations used to generate equivalent atoms: A: 1-x, 1-y, 2-z; B: 1+x, 1+y, z. Although the distances between two benzene planes are close, these planes are not overlapped at all, thus, there are no π-π interactions between two adjacent {Mn$_2$} dimers.

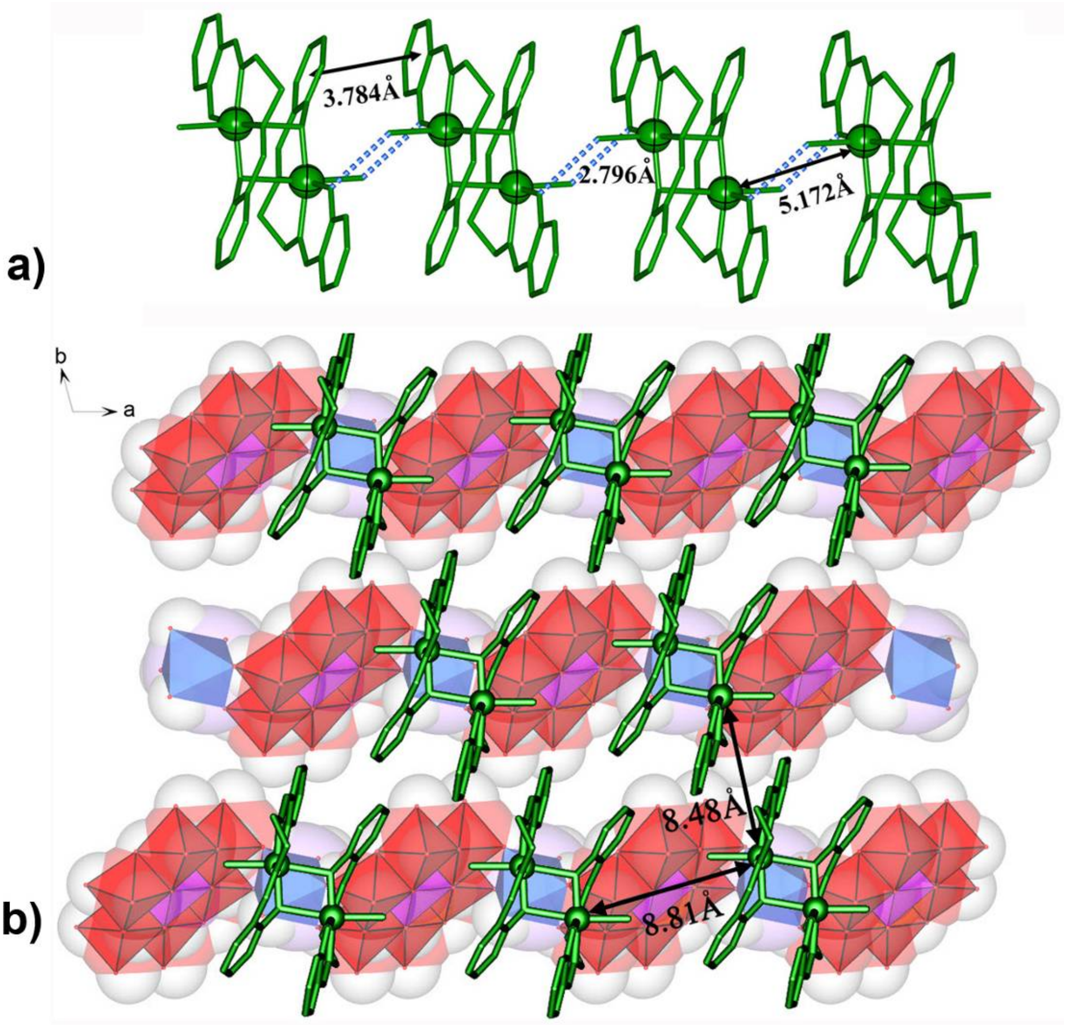

Fig. S11. (a) The 1-D supramolecular chain based on $\{Mn^{III}{}_2\}$-salen moieties extended along *a* axis in 150 the $[Mn_2(salen)_2(H_2O)_2](ClO_4)_2 \cdot H_2O$ precursor (*Chem. Commun.,* 1991, 728); (b) The packing arrangement of $[Mn_2(salen)_2(H_2O)_2]^{2+}$ units on the *a*+*b* plane in **2**.

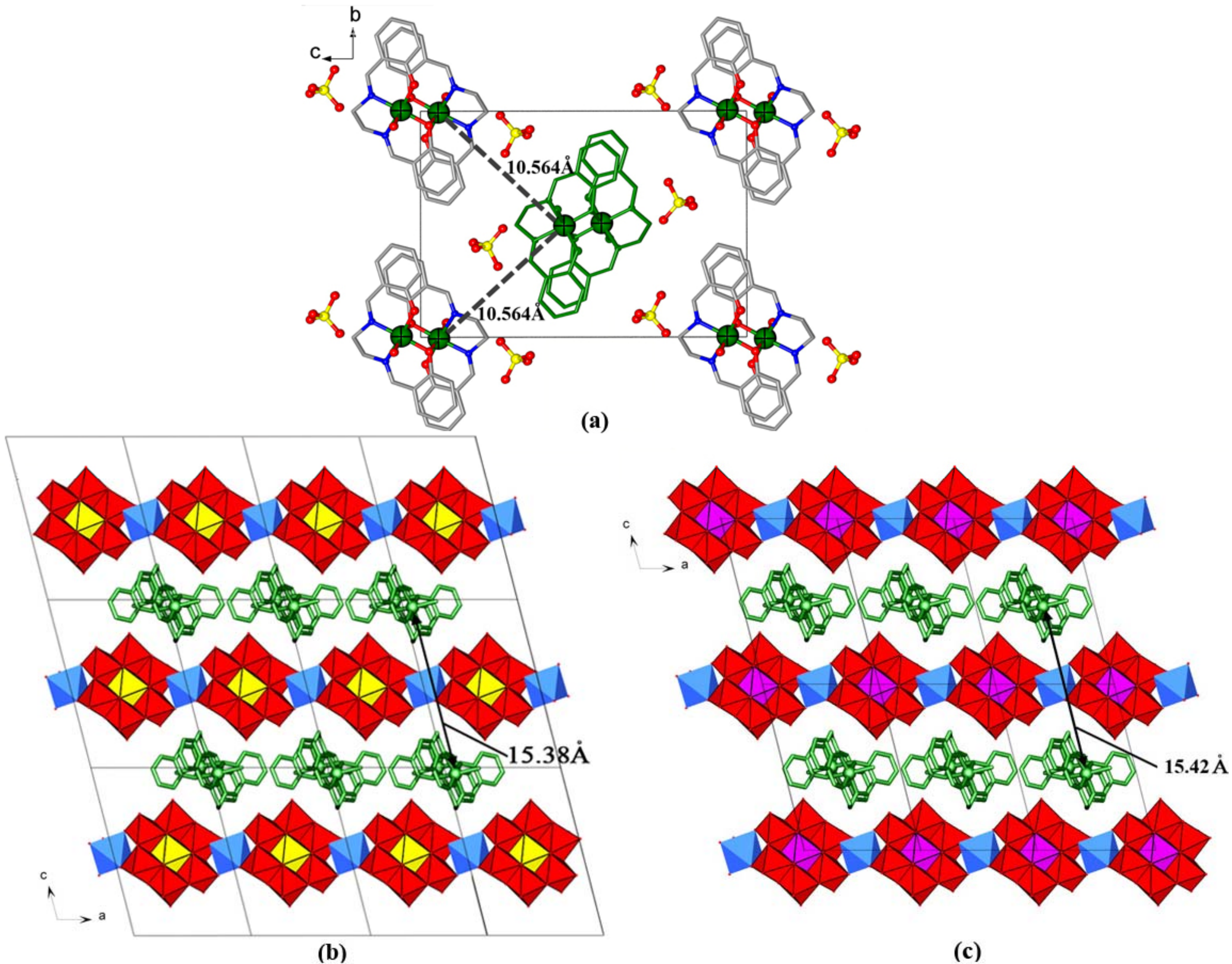

Fig. S12. (a) The packing arrangement of $[Mn^{III}(salen)(H_2O)]_2(ClO_4)_2 \cdot H_2O$ precursor (*Chem.Commun.,* 1991, 728) viewed along a axis. The interdimer separations are both 10.564 Å. H atoms and solvent water molecules are omitted for clarity; (b) and (c) represent the packing arrangement of **1** and **2** viewed along *b* axis. The interdimer separations of packing arrangement for **1** and **2** are 15.38 Å and 15.342 Å, separately.

3 Tables

Table S1 Crystal Data and Structure Refinement for **1** and **2**

	1	**2**
Empirical formula	$C_{32}H_{78}N_4O_{50}Mn_2AlMo_6Na$	$C_{32}H_{78}N_4O_{50}Mn_2CrMo_6Na$
M /g mol^{-1}	2054.47	2079.49
λ /Å	0.71073	0.71073
T /K	150(2)	150(2)
Crystal dimensions /mm	0.29 × 0.27 × 0.24	0.28 × 0.26 × 0.23
Crystal system	Triclinic	Triclinic
Space group	*P-1*	*P-1*
a /Å	10.860(2)	10.896(2)
b /Å	11.219(2)	11.223(2)
c /Å	15.377(3)	15.417(3)
α /°	105.62(3)	105.47(3)
β /°	98.15(3)	98.24(3)
γ /°	109.04(3)	109.18(3)
V /Å^3	1650.4(6)	1660.0(6)
Z	1	1
D_c /g cm^{-3}	2.067	2.080
μ /mm^{-1}	1.606	1.738
F(000)	1024	1035
θ Range /°	3.06 – 25.00	3.05 – 25.00
Reflections collected / unique	12709 / 5566	12844 / 5772
R_{int}	0.0571	0.0240
Data/restraints/parameters	5566 / 69 / 520	5772 / 63 / 520
Goodness-of-fit on F^2	1.049	1.063
R_1 ($I > 2\sigma(I)$)^a	0.0470	0.0266
wR_2 (all data)^b	0.1086	0.0681
$\Delta\rho_{\mathrm{max,\ min}}$/ e Å^{-3}	0.811, -0.958	0.667, -0.775

$^aR_1 = \sum||F_0|-|F_C||/\sum|F_0|$; $^bwR_2 = \sum[w(F_0^2-F_C^2)^2]/\sum[w(F_0^2)^2]^{1/2}$

Table S2 Selected bond lengths (Å) and angles (°) of **1**

Mo(1)-O(21)	1.700(5)	Al(1)-O(11)	1.895(5)
Mo(1)-O(14)	1.719(5)	Al(1)-O(11)#1	1.895(5)
Mo(1)-O(22)	1.931(5)	Al(1)-O(12)#1	1.896(4)
Mo(1)-O(16)	1.944(5)	Al(1)-O(12)	1.896(4)
Mo(1)-O(12)	2.243(5)	Al(1)-O(13)	1.904(5)
Mo(1)-O(13)	2.273(4)	Al(1)-O(13)#1	1.904(5)
Mo(2)-O(19)	1.704(5)	Mn(1)-O(2)	1.867(5)
Mo(2)-O(15)	1.711(5)	Mn(1)-O(1)	1.922(5)
Mo(2)-O(22)	1.922(5)	Mn(1)-N(1)	1.966(6)
Mo(2)-O(20)	1.926(5)	Mn(1)-N(2)	1.976(6)
Mo(2)-O(11)	2.291(5)	Mn(1)-O(1W)	2.190(5)
Mo(2)-O(13)	2.336(5)	Mn(1)-O(1)#2	2.348(5)
Mo(3)-O(18)	1.698(5)	O(14)-Na(1)	2.404(5)
Mo(3)-O(17)	1.715(5)	O(15)-Na(1)	2.370(5)
Mo(3)-O(16)#1	1.918(5)	Na(1)-O(15)#3	2.370(5)
Mo(3)-O(20)	1.937(5)	Na(1)-O(31)	2.372(5)
Mo(3)-O(11)	2.293(5)	Na(1)-O(31)#3	2.372(5)
Mo(3)-O(12)#1	2.319(5)	Na(1)-O(14)#3	2.404(5)
O(2)-Mn(1)-O(1)	96.0(2)	O(1)-Mn(1)-O(1W)	91.4(2)
O(2)-Mn(1)-N(1)	172.4(2)	N(1)-Mn(1)-O(1W)	93.7(2)
O(1)-Mn(1)-N(1)	90.0(2)	N(2)-Mn(1)-O(1W)	95.5(2)
O(2)-Mn(1)-N(2)	92.2(2)	O(2)-Mn(1)-O(1)#2	91.20(18)
O(1)-Mn(1)-N(2)	169.1(2)	O(1)-Mn(1)-O(1)#2	79.05(19)
N(1)-Mn(1)-N(2)	81.3(2)	N(1)-Mn(1)-O(1)#2	85.3(2)
O(2)-Mn(1)-O(1W)	90.9(2)	N(2)-Mn(1)-O(1)#2	93.7(2)
O(1W)-Mn(1)-O(1)#2	170.4(2)		

Symmetry transformations used to generate equivalent atoms: #1 -x+1,-y+1,-z+;#2 -x+2,-y+1,-z+2; #3 -x+2,-y+1,-z+1

Table S3 Selected bond lengths (Å) and angles (°) of **2**

Mo(1)-O(20)	1.703(2)	Cr(1)-O(12)#1	1.969(2)
Mo(1)-O(18)	1.714(2)	Cr(1)-O(12)	1.969(2)
Mo(1)-O(14)	1.924(2)	Cr(1)-O(13)	1.970(2)
Mo(1)-O(22)	1.946(2)	Cr(1)-O(13)#1	1.970(2)
Mo(1)-O(13)	2.288(2)	Cr(1)-O(11)#1	1.971(2)
Mo(1)-O(12)	2.314(2)	Cr(1)-O(11)	1.971(2)
Mo(2)-O(15)	1.709(2)	Na(1)-O(21)#4	2.383(3)
Mo(2)-O(19)	1.715(2)	Na(1)-O(31)#4	2.387(3)
Mo(2)-O(16)#1	1.930(2)	Na(1)-O(31)	2.387(3)
Mo(2)-O(14)	1.948(3)	Na(1)-O(19)#5	2.414(3)
Mo(2)-O(12)	2.246(2)	O(19)-Na(1)#2	2.414(3)
Mo(2)-O(11)	2.278(2)	O(21)-Na(1)	2.383(3)
Mo(3)-O(17)	1.702(2)	Mn(1)-O(1)	1.879(2)
Mo(3)-O(21)	1.713(3)	Mn(1)-O(2)	1.921(2)
Mo(3)-O(22)	1.924(2)	Mn(1)-N(2)	1.976(3)
Mo(3)-O(16)	1.936(2)	Mn(1)-N(1)	1.977(3)
Mo(3)-O(13)	2.287(2)	Mn(1)-O(1W)	2.194(3)
Mo(3)-O(11)#1	2.328(3)	Mn(1)-O(2)#3	2.355(2)
O(1)-Mn(1)-O(2)	95.90(10)	O(2)-Mn(1)-O(1W)	91.86(11)
O(1)-Mn(1)-N(2)	172.72(12)	N(2)-Mn(1)-O(1W)	93.29(11)
O(2)-Mn(1)-N(2)	89.94(11)	N(1)-Mn(1)-O(1W)	94.89(12)
O(1)-Mn(1)-N(1)	92.04(11)	O(1)-Mn(1)-O(2)#3	91.48(10)
O(2)-Mn(1)-N(1)	169.50(11)	O(2)-Mn(1)-O(2)#3	79.04(10)
N(2)-Mn(1)-N(1)	81.66(12)	N(2)-Mn(1)-O(2)#3	85.34(10)
O(1)-Mn(1)-O(1W)	90.87(11)	N(1)-Mn(1)-O(2)#3	93.92(11)
		O(1W)-Mn(1)-O(2)#3	170.79(10)

Symmetry transformations used to generate equivalent atoms:#1 -x,-y,-z+1;#2 x-1,y,z; #3 -x+1,-y,-z+2;#4 -x+1,-y,-z+1;#5 x+1,y,z

Table S4 Pertinent bond distances (Å) and angles (°) for the out-of-plane dimeric cores (F = ferromagnetic interaction, AF = antiferromagnetic interaction)

	Mn-O	Mn-O*	O-Mn-O*	Mn-O-Mn*	Mn…Mn*		ref
1	1.922(5)	**2.348(5)**	79.05(19)	100.95(19)	**3.305(4)**	F	This work
2	1.921(2)	**2.355(2)**	79.04(10)	100.96(10)	**3.310(4)**	F	This work
a	1.901(5)	**2.412(6)**	79.42(21)	100.58(22)	**3.334(3)**	F	[1]
b	1.891(3)	**2.490(3)**	80.7(1)	99.3(1)	**3.361(2)**	AF	[2]
c	1.880(6)	**2.750(6)**	81.3(2)	98.7(2)	**3.558(3)**	AF	[3]

[a] $[Mn(salen)(H_2O)]_2(ClO_4)_2$. [b] $[Mn(salen)(H_2O)]_2(ClO_4)_2 \cdot H_2O$. [c] [Mn(salen)(NCS)].

References:

[1] H.-L. Shyu, H.-H. Wei and Y. Wang, *Inorg. Chim. Acta*, 1999, **290**, 8.
[2] A. Garcia-Deibe, A. Sousa, M. R. Bermejo, P. P. MacRory, C. A. McAuliffe, R. G. Pritchard and M. Hellowell, *J. Chem. Soc., Chem. Commun.*, 1991, 728.
[3] M. Mikuriya, Y. Yamato and T. Tokii, *Bull. Chem. Soc. Jpn.*, 1992, **65**, 1466.

Table S5. Magnetic parameters of compound **1**, **2** and **3** as well as several Mn(III) dimeric SMMs (n = no data in the literature)

Compound	g	J/k_B (K)	zJ' (K)	D_{Mn}/k_B (K)	$\lvert D_{ST} \rvert S_T^2$ (K)[d]	□ τ_0 (S) (T > 1.8 K)[d]	Ref.
$[Mn(salen)(H_2O)]_2Na[AlMo_6(OH)_6O_{18}]\bullet 20H_2O$[a]	1.98(2)	+0.89(2)	-0.03(1)	n	13.2	7.2×10^{-7} (H_{dc} = 700 Oe)	**1**
$[Mn(salen)(H_2O)]_2Na[CrMo_6(OH)_6O_{18}]\bullet 20H_2O$[a]	1.92(2)	+0.63(2)	-0.04(1)	n	9.1	16×10^{-7} (H_{dc} = 600 Oe)	**2**
$[Mn(salen)(H_2O)]_2(ClO_4)_2\bullet H_2O$[a]	1.97(2)	+2.12(5)	-0.26	n	n	n	**3**
$[Mn(saltmen)(ReO_4)]_2$[b]	2.00(1)	+2.57	-0.2	-1.59	16	8×10^{-9} (H_{dc} = 0 Oe)	14(a)
$[Mn(saltmen)(O_2CCH_3)]_2$[b]	1.98	+1.95	n	-2.74	27.8	5.1×10^{-8} (H_{dc} = 5000 Oe)	14(c)
$[Mn(saltmen)(N_3)]_2$[b]	1.98	+0.86	n	-1.44	28.7	1.0×10^{-8} (H_{dc} = 1000 Oe)	14(c)
$[Mn(salen)(NCO)]_2$[b]	2.03	+1.05	n	-0.43	23.5	2.3×10^{-8} (H_{dc} = 1000 Oe)	14(c)
[Mn(3,5-Brsalen)(3,5-Brsalicylaldehyde)]$_2$[b]	2.00	+0.79	n	-5.91	22.5	4.6×10^{-8} (H_{dc} = 1000 Oe)	14(c)
$[Mn(ins)(\mu_{1,1}\text{-}N_3)(CH_3OH)]_2$[c]	2.01	+5.00	n	-13.18	n	n	14(e)
$[Mn(L)(N_3)]_2$[a,b]	2.03	+0.85	-0.029	-2.16	n	n	**e**

a. The parameters of g, J/K_B and zJ' are obtained from the isotropic Heisenberg dimer model of S = 2 spins considering the inter-dimer magnetic interaction (zJ'). See the ESI text in P19 and the reference **e**.

b. The parameters of g, J/K_B and D_{Mn}/k_B are obtained from the model below[14a,c] and their units are unified in order to compare with each other.

$$H = -2JS_1S_2 + D_{Mn}\sum_{i=1,2} S_{iz}^2 + g\mu_B H \sum_{i=1,2} S_i$$

c. The parameters of g, J/K_B and D_{Mn}/k_B are obtained from the model below[14e] and their units are unified in order to compare with each other.

$$H = S_1 \cdot J \cdot S_2 + \sum_{i=1}^{2} (S_i \cdot D_i \cdot S_i + \mu_B B \cdot g_i \cdot S_i)$$

d. The activation energy and relaxation time (τ_0) are obtained from the plots of relaxation time τ versus 1/T following the Arrhenius law ($\tau = \tau_0 \exp(E_a/K_BT)$).

e. S. Mandal, G. Rosair, J. Ribas and D. Bandyopadhyay, *Inorg. Chim. Acta*, 2009, **362**, 2200.

4 Magnetic Properties of 1 and 2 as well as the $[Mn^{III}_2(salen)_2(H_2O)_2](ClO_4)_2{\cdot}H_2O$ precursor

1) Magnetic properties of the $[Mn^{III}_2(salen)_2(H_2O)_2](ClO_4)_2{\cdot}H_2O$ precursor.

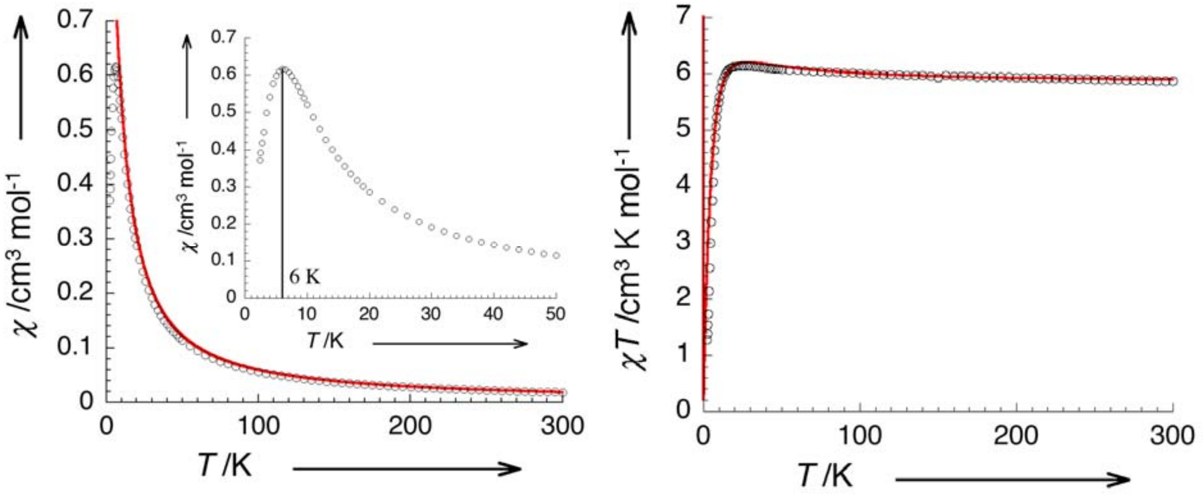

Fig. S13. The temperature dependence of (left) the magnetic susceptibility χ (being defined as M/H per $[Mn_2]$ dinuclear unit) and (right) χT product for $[Mn^{III}_2(salen)_2(H_2O)_2](ClO_4)_2{\cdot}H_2O$ (**3**) under 0.1 T. The red lines represent the best fit using an isotropic Heisenberg $S_{Mn} = 2$ dimer model including inter-complex magnetic interactions treated in the frame of the mean field theory (see text).

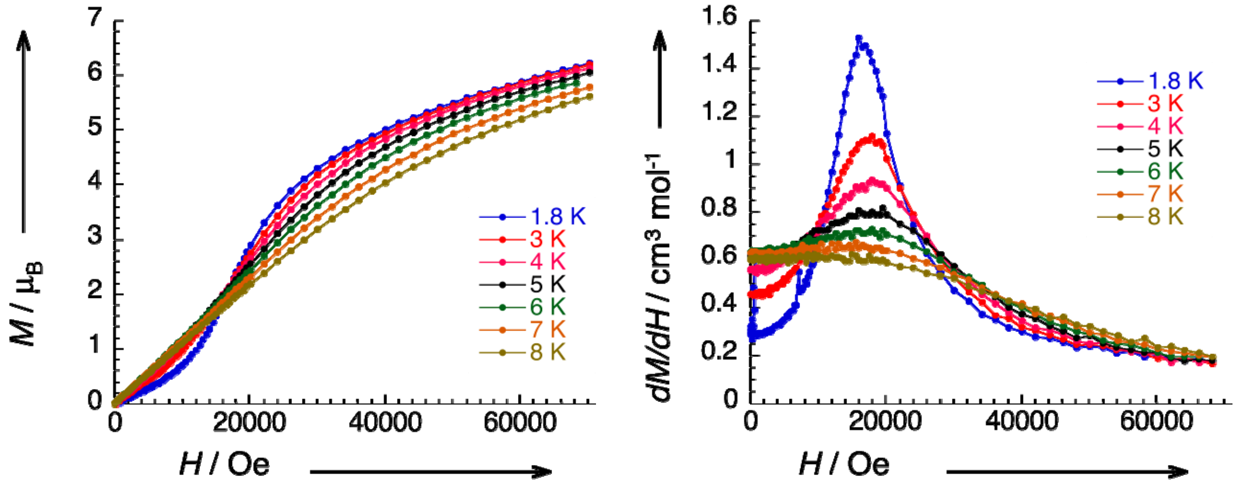

Fig. S14. Field dependence of (left) the magnetization (M) and (right) the field derivative of M (dM/dH) at different temperatures for $[Mn^{III}_2(salen)_2(H_2O)_2](ClO_4)_2{\cdot}H_2O$ (**3**) emphasizing the present of significant antiferromagnetic interactions between Mn(III) dinuclear moieties that lead to an antiferromagnetic order below 6 K. Solid lines are guides for the eyes.

2) Magnetic properties of 1 and 2.

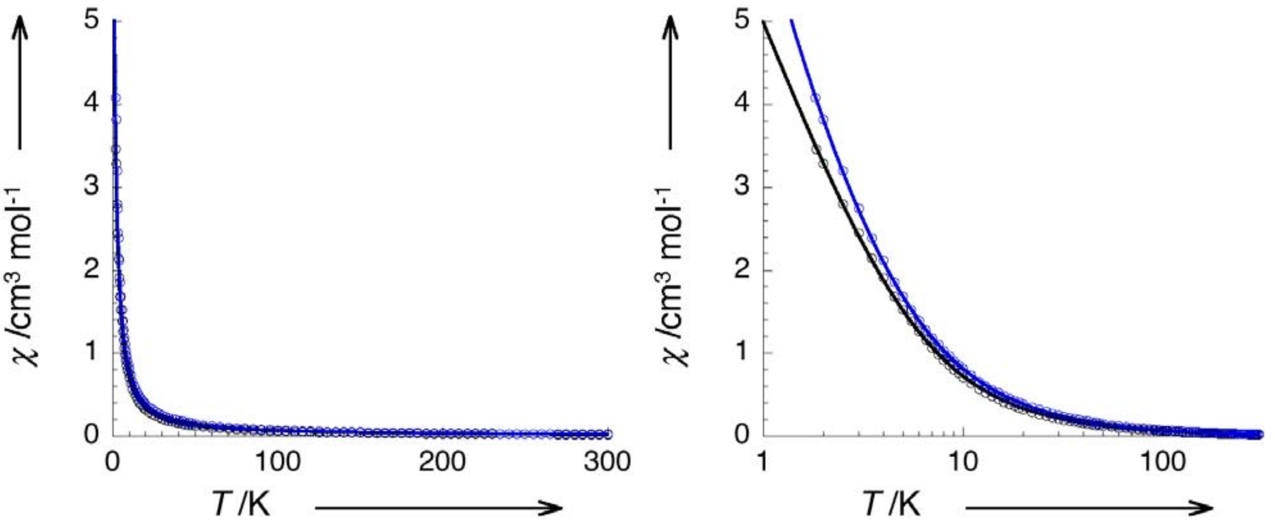

Fig. S15. The temperature dependence of the magnetic susceptibility χ (being defined as M/H per [Mn_2] dinuclear unit; left in linear scales and right in semi-logarithm plot) for **1** (in black) and **2** (in blue) under 0.1 T. The solid lines represent the best fit using an isotropic Heisenberg $S_{Mn} = 2$ dimer model including inter-complex magnetic interactions treated in the frame of the mean field theory (see text).

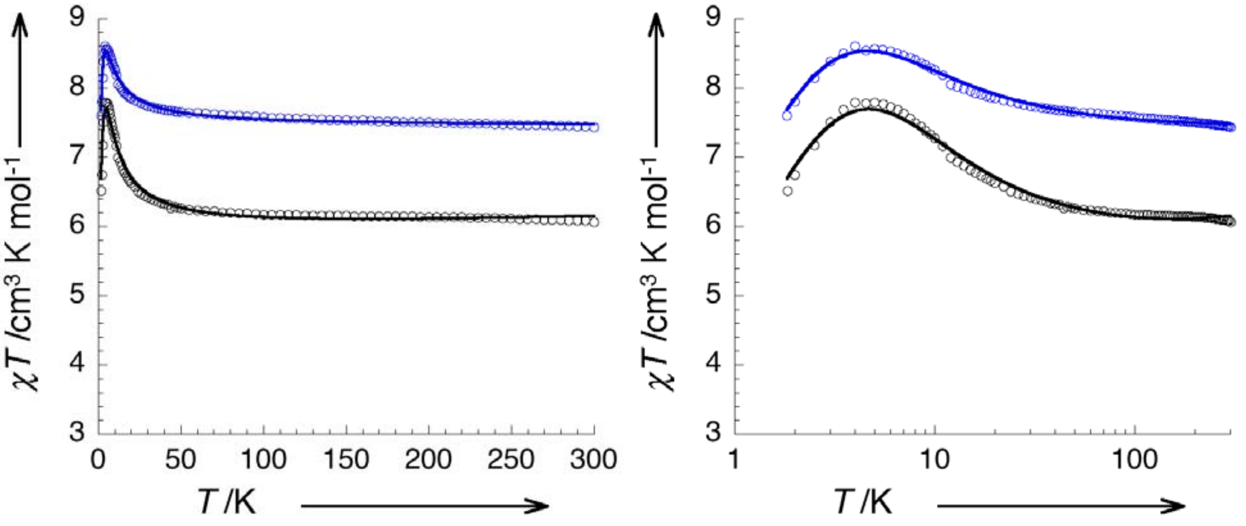

Fig. S16. The temperature dependence of the χT product (per [Mn_2] dinuclear unit; left in linear scales and right in semi-logarithm plot) for **1** (in black) and **2** (in blue) under 0.1 T. The solid lines represent the best fit using an isotropic Heisenberg $S_{Mn} = 2$ dimer model including inter-complex magnetic interactions treated in the frame of the mean field theory (see text).

The dc magnetic susceptibilities of **1**, **2** and **3** were measured on polycrystalline samples in the temperature range of 1.8 to 300 K at 0.1 T (Fig. S13 and S15). For the three compounds, the χT product increases when the temperature is lowered from 300 to 8 K revealing the presence of intra-complex Mn^{III}-Mn^{III} ferromagnetic interactions as already observed in analogous systems.[21,22] At lower temperatures, the decrease of χT product is observed for all the compounds (Fig. S13 and S15) as a signature of the magnetic anisotropy brought by the $\mathrm{Mn^{III}}$ metal ions but also likely due to the presence of inter-molecular antiferromagnetic interactions between adjacent $\{\mathrm{Mn_2}\}$ units. The presence of significant antiferromagnetic interactions is clearly observed in the precursor **3** by (i) the very marked low temperature drop of the χT product in comparison to **1** and **2** and (ii) also a maximum on the χ vs T data (absent for **1** and **2**) that suggests the presence of antiferromagnetic order below 6 K. The M vs H data of **3** measured between 8 and 1.8 K (Fig. S14) display a typical *S*-shape curve below 6 K (also seen as a maximum on the dM/dH vs H plot, Fig. S14) and further support this hypothesis. Therefore complex **3** does not display any sign of SMM properties above 1.8 K due to the presence of strong inter-molecular interactions that stabilize an antiferromagnetic order below 6 K.

The room temperature χT products of compounds **1** and **2** are in good agreement with the expected values (6.0 and 7.875 $\mathrm{cm^3.K/mol}$) for two $\mathrm{Mn^{III}}$ metal ions ($S = 2$, $g = 2$) in **1** and two $\mathrm{Mn^{III}}$ and one $\mathrm{Cr^{III}}$ ($S = 3/2$, $g = 2$) metal ions in **2**. Considering dinuclear structure of the compounds, their temperature dependence of the magnetic susceptibility has modelled using a simple isotropic Heisenberg dimer model of $S = 2$ spins with the following spin Hamiltonian: $H = -2JS_{MnA}S_{MnB}$, where J is the exchange interactions in the dimer between Mn(III) ions. It is worth noting that the magnetic anisotropy and the inter-molecular interactions have been neglected in this approach. The application of the van Vleck equation[1] to the Kambe's vector coupling scheme,[2] allows a determination of the low field analytical expression of the magnetic susceptibility:

$$\chi_0 = \frac{g_{av}^2 N \mu_B^2}{k_B T} \frac{2e^{\frac{2J}{k_B T}} + 10e^{\frac{6J}{k_B T}} + 28e^{\frac{12J}{k_B T}} + 60e^{\frac{20J}{k_B T}}}{1 + 3e^{\frac{2J}{k_B T}} + 5e^{\frac{6J}{k_B T}} + 7e^{\frac{12J}{k_B T}} + 9e^{\frac{20J}{k_B T}}}$$

Two additional ingredients were included in the model: (i) an additional $S = 3/2$ Curie law was included in order to fit the data for **2** (that contains an isolated $S = 3/2$ $\mathrm{Cr^{III}}$ in the POM core) and (ii) inter-dimer magnetic interaction (zJ') was introduced in the frame of the mean-field approximation to simulate adequately the low temperature χT products for both compound (below 6 K).[3] The following definition of the susceptibility has been used for the mean field approach:

$$\chi = \frac{\chi_0}{1 - \frac{2zJ'}{Ng^2\mu_B^2}\chi_0}$$

where χ_0 is the susceptibility of the isolated dimers, z the number of nearest neighbors and J' the magnetic interactions between units.[3] Very good fits of the data have been achieved using $J/k_B =$

+0.89(2) K, zJ'/k_B = -0.03(1) K and g = 1.98(2) for **1** and J/k_B = +0.63(2) K, zJ'/k_B = -0.04(1) K and g = 1.92(2) for **2**.

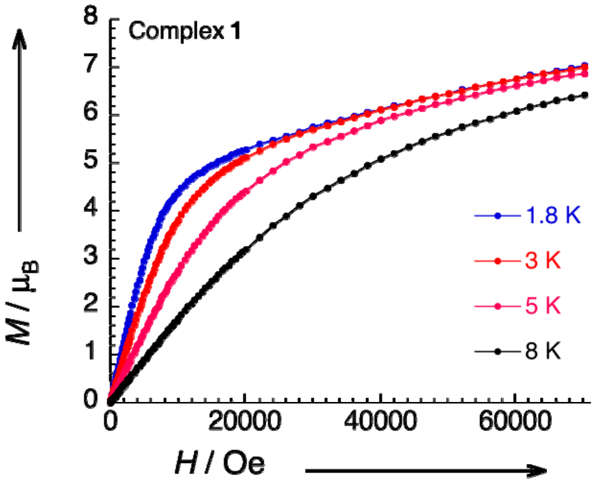

Fig. S17. Field dependence of magnetization below 8 K for **1** (left) and **2** (right).

For both compounds, the field dependence of the magnetization below 8 K reveals a relative rapid increase of the magnetization at low fields and then a very slow linear increase without a clear saturation even at 7 T and 1.8 K (as shown in Fig. S17). The magnetization at 1.8 K and 7 T is 7.0 and 9.1 μ_B for **1** and **2**, respectively. The high field linear variation of the magnetization suggests the presence of a significant magnetic anisotropy.

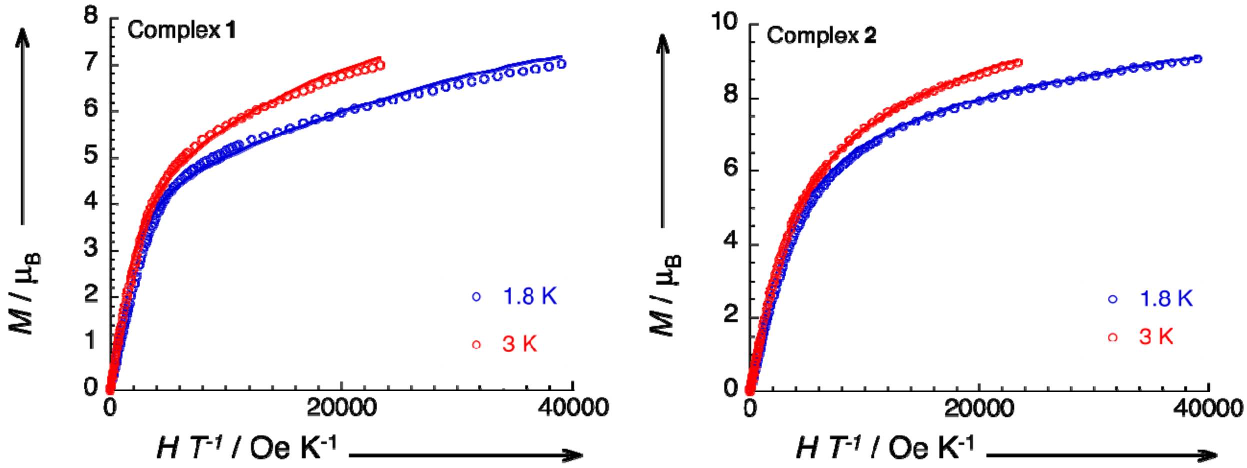

Fig. S18. M vs H/T plot below 3 K for **1** (left) and **2** (right). The solid lines represent the best fits using an anisotropic Heisenberg $S_T = 4$ model with the following Hamiltonian: $H = DS_{T,z}^2$ (see text).

Moreover, while plotting the M vs H/T (as shown in Fig. S18) at different fields, the curves are not all superposed on a single master-curve further indicating the presence of magnetic anisotropy. Therefore these data have been fitted to an anisotropic Heisenberg $S_T = 4$ model with the following

Hamiltonian: $H = DS_{T,z}^2$ (note that for **2**, an $S = 3/2$ Brillouin function with $g = 2$ has been added to the model to take into account the contribution from the Cr(III) metal ions of the $[CrMo_6(OH)_6O_{18}]^{3-}$ anionic POM). Due to the weak intra-complex ferromagnetic interactions, only the data below 3 K can be fit in a reasonable manner with $D/k_B = -1.0(2)$ K and $g = 2.01(5)$ for **1** and $D/k_B = -1.3(2)$ K and $g = 1.86(5)$ for **2** (Fig. S18).

In addition, it is worth noting that no hysteresis effect on the *M* vs *H* data has been observed above 1.8 K with sweep-rate used in a traditional SQUID magnetometer (100 – 200 Oe/min) for both compounds.

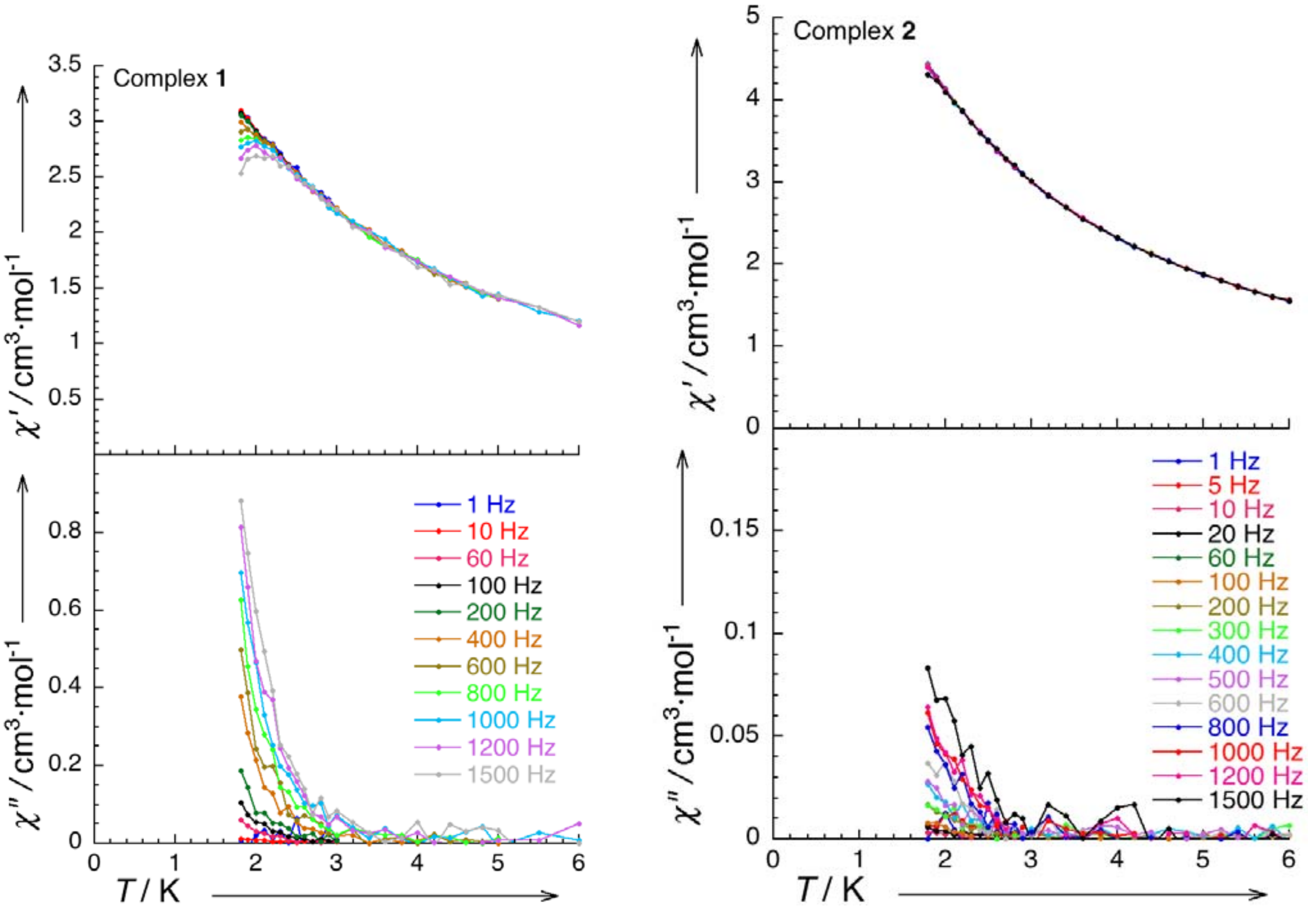

Fig. S19. Temperature and frequency dependence of the real (χ') and imaginary (χ'') parts of the ac susceptibility for **1** (left) and **2** (right) in zero dc field and with a 3 Oe ac field. Solid lines are guides for the eyes.

The ac susceptibility of these complexes in zero dc-field have been checked. Clearly at low temperatures below 3 K (for frequency around 1500 Hz), slow relaxation of the magnetization is observed based on the appearance of a weak out-of-phase signal as shown in Fig. S19. These features (shape and frequency dependence) suggests that these compounds are SMMs as previously reported dinuclear Mn^{III} complexes.[4] In these systems, the slow relaxation of the magnetization and its associate relaxation time are too fast to be followed by ac technique with frequency between 1 and 1500 Hz due to the fast quantum relaxation in zero field. In order to short-cut the fast quantum relaxation in zero-field (that explains the lack of hysteresis *M* vs *H* loop in zero field) and to probe the quantum contribution to the observed relaxation above 1.8 K, a dc-field has been applied and the ac susceptibility measured. As expected when quantum relaxation is effective, the relaxation rate is slow down very dramatically at 1.8 K for both compounds as shown in Fig. S20.

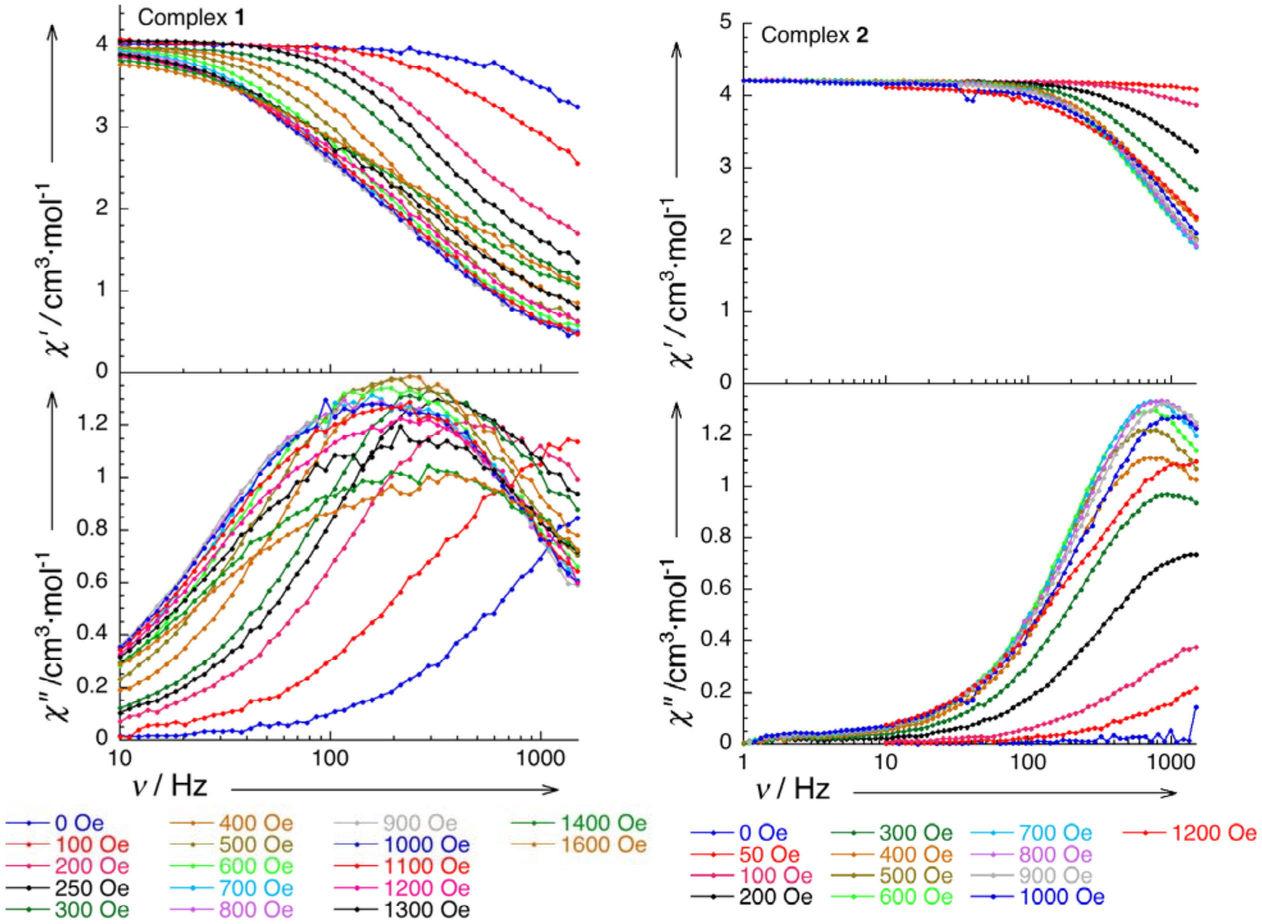

Fig. S20. Frequency dependence of the real (χ') and imaginary (χ'') parts of the ac susceptibility for **1** (left) and **2** (right) at 1.8 K in different dc field and with a 3 Oe ac field. Solid lines are guides for the eyes.

From these measurements, one can extract the relaxation time of the magnetization as a function of the applied field as shown in Fig. S21. The quantum effects seem to be minimized around 700 or 600 Oe as shown in Fig. S21 by the minimum of the characteristic frequency of the system observed at 1.8 K for **1** and **2,** respectively. Therefore measuring the ac susceptibility at 700 Oe for **1** and 600 Oe for **2** at different temperatures allow to determine the relaxation time mainly dominated by the thermal effects above 1.8 K as shown in Fig. S22 and Fig. S23. At these fields, the temperature dependence of the relaxation time has been deduced for both compounds as described in the main text.

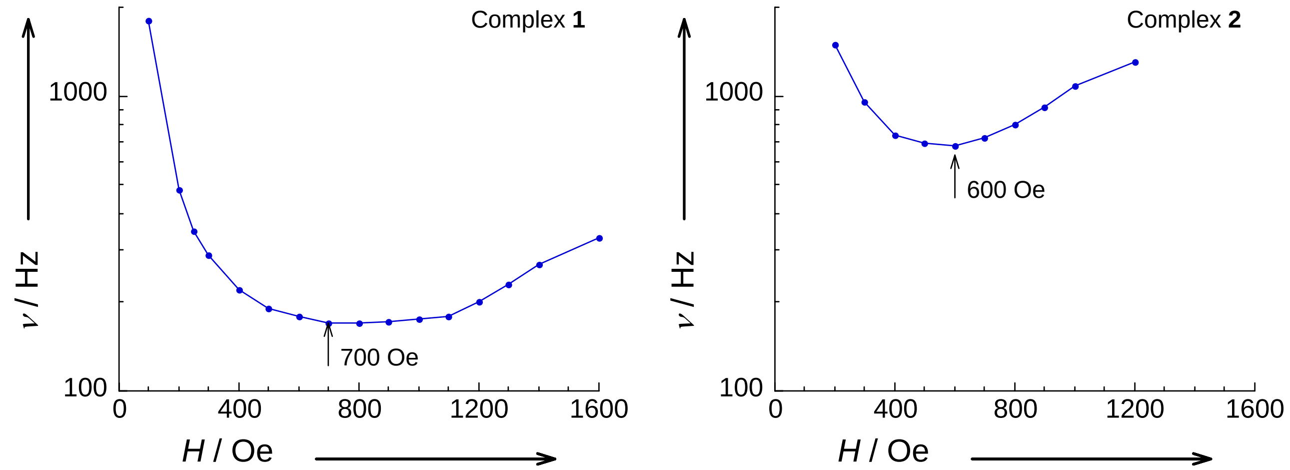

Fig. S21. Field dependence of the characteristic relaxation frequency for **1** (left) and **2** (right) at 1.8 K. Solid lines are guides for the eyes.

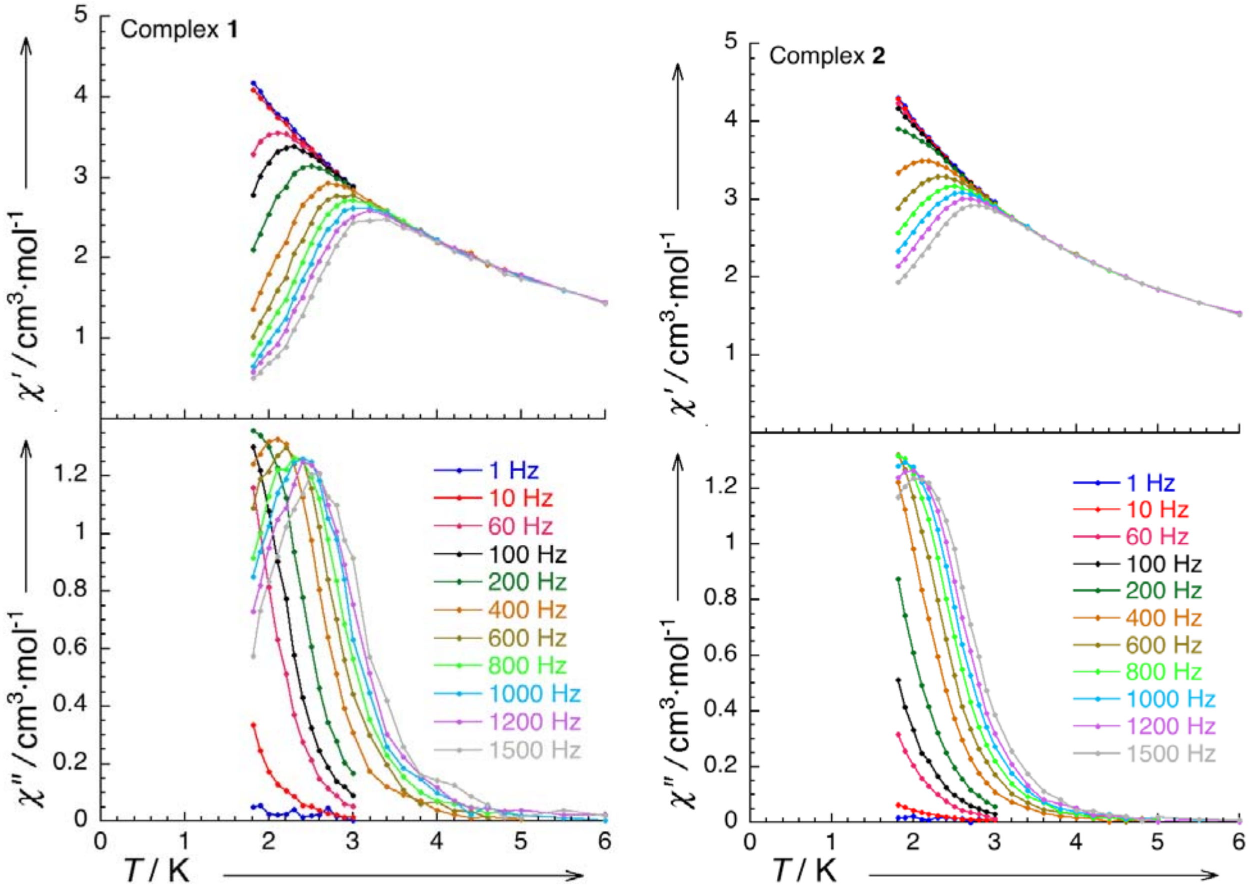

Fig. S22. Temperature dependence of the real (χ') and imaginary (χ'') parts of the ac susceptibility for **1** (left) and **2** (right) at different frequencies at 700 and 600 Oe respectively and with a 3 Oe ac field. Solid lines are guides for the eyes.

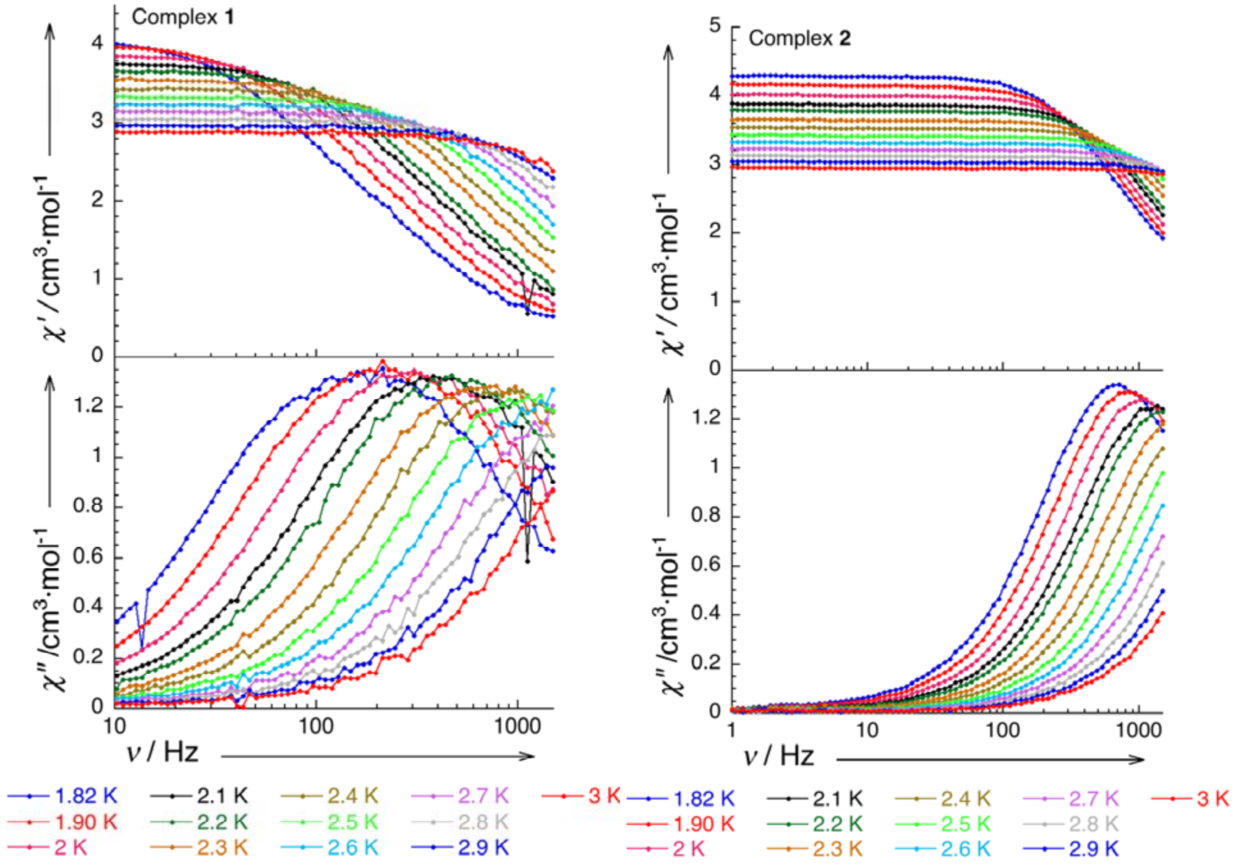

Fig. S23. Frequency dependence of the real (χ') and imaginary (χ'') parts of the ac susceptibility for **1** (left) and **2** (right) at different temperatures at 700 and 600 Oe respectively and with a 3 Oe ac field. Solid lines are guides for the eyes.

References:

1 J. H. van Vleck, *The Theory of Electric and Magnetic Susceptibility*, Oxford University Press, 1932.

2 K. Kambe, *J. Phys. Soc. Jpn.* 1950, 5, 48.

3 (a) B. E. Myers, L. Berger and S. Friedberg, *J. Appl. Phys.*, 1969, **40**, 1149; (b) C. J. O'Connor, *Prog. Inorg. Chem.*, 1982, **29**, 203.

4 (a) H. Miyasaka, R. Clérac, W. Wernsdorfer, L. Lecren, C. Bonhomme, K.-i. Sugiura and M. Yamashita, *Angew. Chem. Int. Ed.*, 2004, **43**, 2801.

5. Other characterizations of 1 and 2

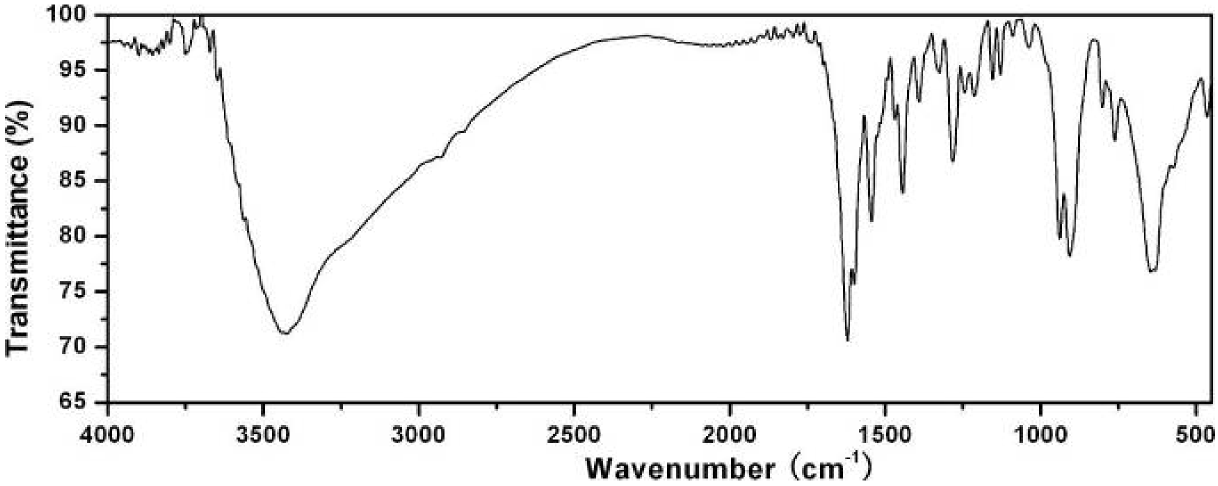

Fig. S11. IR spectrum of **1**

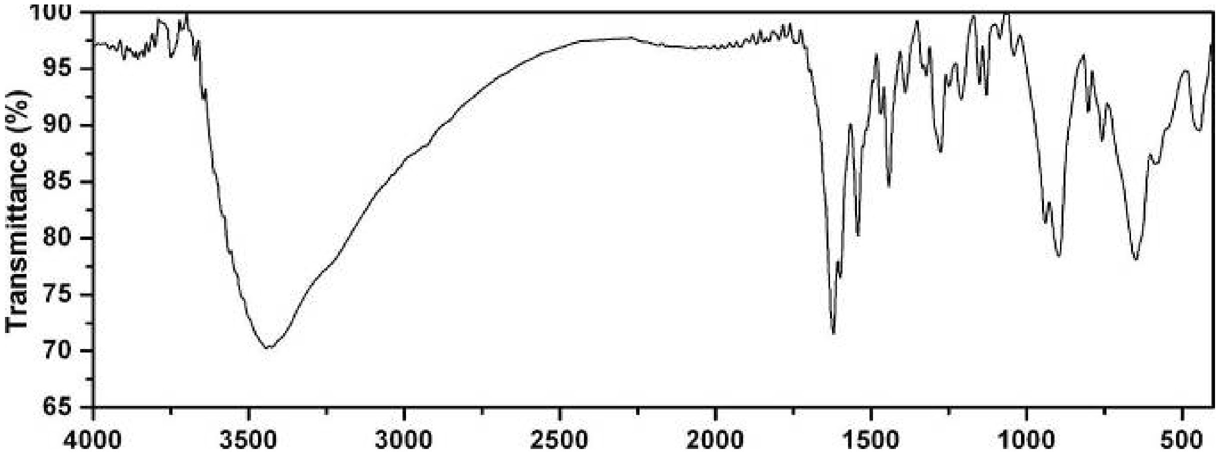

Fig. S12. IR spectrum of **2**

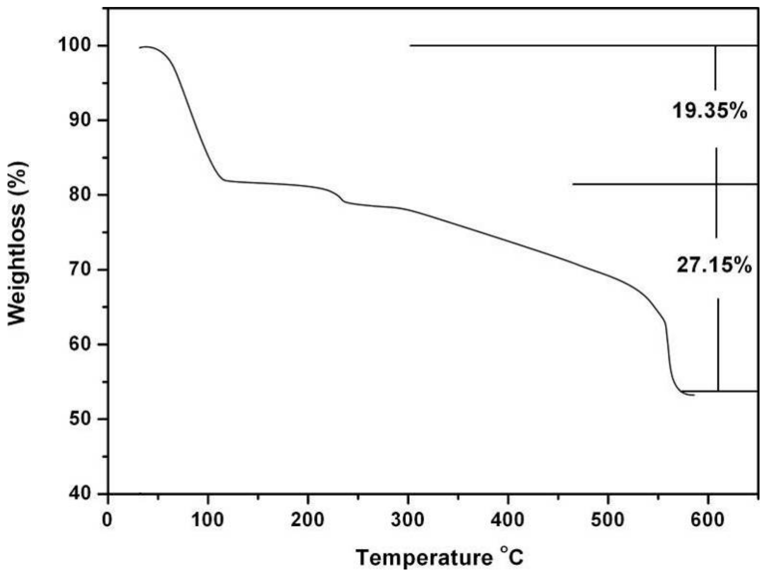

Fig. S13. TG curve of **1**

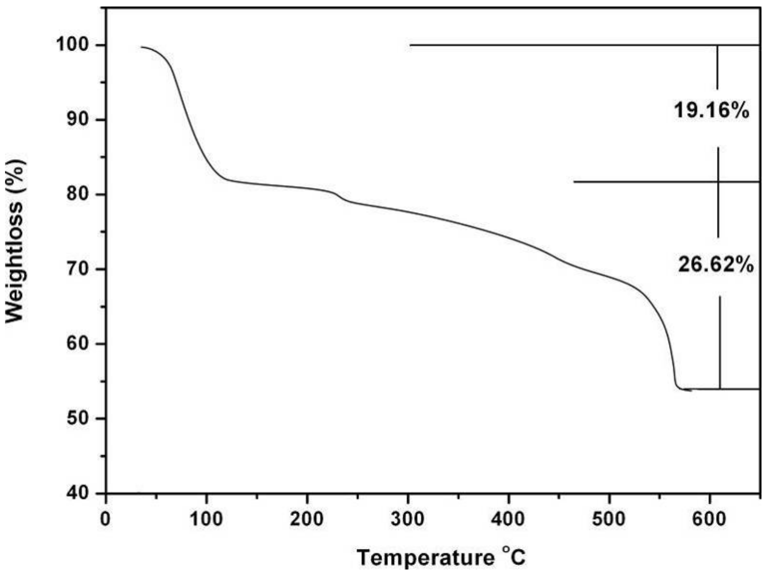

Fig. S14 TG curve of **2**

TG discussion: The TG curves of both complexes show three weight loss steps. The first two weight loss steps in the temperature range of 40 - 240 ºC are attributed to the loss of lattice and coordinated water molecules (found: 19.35%, calc: 19.27 % for **1** and found: 19.16%, calc: 19.04 for **2**). The third weight loss occurs from 300 ºC to 570 ºC, which is assigned to the decomposition of the organic components and the loss of H and O atoms in the water molecule form (found: 27.15%, calc: 25.59 % for **1** and found: 26.62%, calc: 25.92 % for **2**).